



Ratio fluorescent hybrid probe for visualized fluorescence detection of H₂O₂ *in vitro* and *in vivo*

Riyue Dong^{a,b,c}, Yuying Yao^{a,b,c}, Dongna Li^{a,b,c}, Haoran Zhang^{a,b,c}, Wei Li^{a,b,c}, Maxim Molokey^d, Yingliang Liu^{a,b,c}, Bingfu Lei^{a,b,c,*}

^a College of Materials and Energy, South China Agricultural University, Guangzhou 510642, PR China

^b Guangdong Laboratory of Lingnan Modern Agriculture, Guangzhou 510642, PR China

^c Guangdong Provincial Engineering Technology Research Center for Optical Agriculture, Guangzhou 510642, PR China

^d SB RAS, Kirensky Inst Phys, Lab Crystal Phys, Krasnoyarsk 660036, Russia

ARTICLE INFO

Keywords:

Si-O
QDs
Ag
Nanoclusters
Visualized fluorescence detection
H₂O₂ sensing *in vivo* and *in vitro*

ABSTRACT

A silicon oxide quantum dots (Si-O QDs) and Ag nanoclusters hybrid nanosensing probe with dual-emission and small nanocrystals that acts as an “off-on” ratio fluorescent probe for hydrogen peroxide (H₂O₂) detection was developed. The probe was used to measure the H₂O₂ concentration generated by mitochondria *in vitro* via recording the I₄₅₅/I₆₈₀ fluorescence ratio. Furthermore, this hybrid probe was applied to monitor the wound-induced H₂O₂ in lettuce leaf, and realized the visualized fluorescence qualitative detection H₂O₂ *in vivo* via laser scanning confocal microscope. The working mechanism of the probe is also investigated. Inner filter effect (IFE) estimation, Fourier transform infrared (FTIR) spectra and high-resolution transmission electron microscopy (HRTEM) images were applied to study the quenching mechanism and recovering reason of Si-O QDs fluorescence. The results show that the blue fluorescence of Si-O QDs can be quenched by Ag NCs via the IFE and fluorescent resonance energy transfer (FRET) effect. After adding H₂O₂, the surface groups of Ag NCs was changed and the IFE and FRET effects between the Si-O QDs and Ag NCs are disabled, thus the quenched Si-O QDs luminescence can be regularly recovered.

1. Introduction

Hydrogen peroxide (H₂O₂) is a byproduct of aerobic metabolism in mitochondria and chloroplasts [1]. It is an essential molecule for plant, because it acts as signal responding to various environmental stimuli which include drought or waterlogging, temperature changes, salt stress, disease, and plant hormones [1–3]. Furthermore, H₂O₂ is also involved in diverse signal transmitting pathways in plant [4–6]. Changes of the H₂O₂ concentration in plant can illustrate the plant defense processes or cell programmed death. Therefore, monitoring of H₂O₂ in plant is a necessary subject in plant science. Nowadays, electrochemical methods and organic fluorescent dye probes are common way used for *in vivo* and *in vitro* H₂O₂ detection in plant. However, these probes have advantages and disadvantages. For example, Bertotti's group [7] monitored H₂O₂ in *Agave tequilana* leaves by using electrochemical sensors, which can dynamically monitor the concentration changes of H₂O₂ *in situ*. However, the required equipment in these methods is complicated and the electrodes will cause physical wounds on plant.

Furthermore, amplex red (10-acetyl-3,7-dihydroxyphenoxazine) has been reported as highly sensitive probe for H₂O₂ detection, and its detection limit is up to the picomole level [8]. However, this fluorescent dye biosensor is photodegraded easily, and the sensitivity is mostly affected by the pH, as well as the organic dye is expensive. Taking the limitations of above methods into account, biosensors based on fluorescent nanoparticles have attracted much attention because of their small size, operability, inexpensiveness, stability and high sensitivity. Electrochemistry, absorbance and optics properties, as well as surface-enhanced Raman scattering (SERS), are used as signals for nanobiosensors of H₂O₂ detection [9–12]. Therein, using the fluorescence as sensing signal is popular method for H₂O₂ detection because of its simple equipment and strong operability. Furthermore, metal-free quantum dots are ideal materials for H₂O₂ detection benefitting from their stable photoluminescence, well biocompatibility and high sensitivity. Wu and colleagues [13] linked carbon dots with recognition element of H₂O₂ for tracing H₂O₂ in cancer cells. Kar's [14] groups and Jelinek' groups [15] reported two similar ratio fluorescent sensing

* Corresponding author.

E-mail address: leiibf@scau.edu.cn (B. Lei).

<https://doi.org/10.1016/j.snb.2020.128643>

Received 13 June 2020; Received in revised form 22 July 2020; Accepted 23 July 2020

Available online 25 July 2020

0925-4005/© 2020 Elsevier B.V. All rights reserved.

platforms for H₂O₂ detection based on carbon dots and hemin. Silicon quantum dots (SiQDs), a kind of quantum dots basing on monocrystalline silicon, are also used in biosensors for H₂O₂. Label-free SiQDs with high selectivity for glucose in serum samples were synthesized by Yao's group [16]. Wang's group [17] also reported silica nanoparticles doped with fluorescein isothiocyanate (FITC) (FSNPs), and it was used for H₂O₂ detection sensor which needs two step reactions. Firstly, KI is oxidized to I₂ by H₂O₂, next, I₂ could quench the fluorescence of FSNPs. Therefore, quenching intensity could be indicator for H₂O₂. However, these sensors basing on metal free quantum dots either need linking with ligands which is sensitive to H₂O₂, or need the productions of H₂O₂ reaction to affect the fluorescence intensity. In these sensors system, the metal-free quantum dots respond to H₂O₂ indirectly. Label free sensors basing on quantum dots that respond directly to H₂O₂ still need to be explored.

To date, metal nanoclusters, a new kind of luminescent nanomaterial, have got much attention benefiting from their optical, physical and chemical properties [18]. Metal nanoclusters have stable photoluminescence, abundant functional groups, large surface area, well biocompatibility and low toxicity, and thus suit well as biological optical sensing and biological imaging. As reported, silver nanoclusters (Ag NCs) have shown their superior performance in biomacromolecule and inorganic ion detection [19–22]. Meanwhile, Ag NCs show their excellent sensitivity for H₂O₂. The mechanism of H₂O₂ detection by Ag NCs has been demonstrated, in which H₂O₂ can etch Ag NCs and then destroy the Ag NCs scaffolds. Therefore, the fluorescence of Ag NCs can be quenched sharply. It makes the Ag NCs become idea nanosensor for H₂O₂ detection [18,23]. For example, Ag NCs were used as an enhancer for Au NCs fluorescence at 618 nm. The fluorescence of this compound could be quenched by ·OH generated from H₂O₂, which makes the fluorescent change of Au/Ag NCs act as signal for H₂O₂ detection [24]. Ag NCs and other metal nanoparticles have single emission, which means that only one signal could be obtained in H₂O₂ detection.

In order to satisfy the sensitivity of H₂O₂ detection with fluorescent nanoparticles, a method benefitting from two signal ratio fluorescent probe was proposed, nanohybrid system is a common way to get dual-signal fluorescent sensors. Silicon oxide quantum dots (Si-O QDs) are synthesized by using *N*-[3-(trimethoxysilyl)propyl]ethylenediamine (DAMO) as precursor with one-pot hydrothermal method in this research. Ag nanoclusters are prepared based on bovine serum albumin (BSA) protection. Ag NCs is sensitive to H₂O₂, while the as-prepared Si-O QDs is less sensitive. Herein, a two signal ratio fluorescent probe is established based on Ag NCs and Si-O QDs. In this ratio fluorescent hybrid probe system, the emission peak at 455 nm is from Si-O QDs, and Ag NCs have emission peak at 680 nm. Ag NCs could quench the fluorescence of Si-O QDs by inner-filter effect (IFE) and the fluorescent resonance energy transfer (FRET) effect. The two effects keep the as-prepared hybrid probe stable. In the detection of H₂O₂, the quenched emission of Si-O QDs can be recovered progressively, while the fluorescence of Ag NCs is decreased. Therefore, the ratio fluorescence of two nanoparticles could change with the altered H₂O₂ concentrations. It was for that good selectivity and high sensitivity for H₂O₂ detection in the range of 0.008–60 mM can be obtained. Basing the advantages of this hybrid probe, it was applied to detect the H₂O₂ generated by plant mitochondria *in vitro*. Besides, owing to the small size particles of hybrid probe system and its stability, it can be infiltrated into lettuce leaf and realized the visualized fluorescence detection of wound-induced H₂O₂ detection *in vivo*.

2. Materials and experimental

2.1. Materials

All chemicals were commercial and without further purified before using. DAMO, trisodium citrate, silver nitrate, sodium hydroxide, sodium borohydride, sodium silicate, hydrogen peroxide, sucrose,

magnesium chloride, ethylene diamine tetraacetic acid (EDTA), cysteine, potassium chloride, Tris–HCl, monopotassium phosphate and potassium hydroxide were purchased from Macklin. BSA and catalase were purchased from Sangon Biotech. All the metal ions are from metal sulfate purchased from Aladdin. All solutions were prepared with deionized water.

2.2. Instrumentations

The fluorescent spectra were recorded by a F-7000 Hitachi fluorescence spectrofluorometer. The UV-vis absorption spectra were recorded on a Shimadzu UV-2550. The transmission electron microscopy TEM and high-resolution transmission electron microscopy (HRTEM) images were taken on an FEI Tecnai 12 transmission electron microscope and a JEOL-2010 electron microscope, respectively. The Fourier-transform infrared (FTIR) spectra were collected with a Nicolet Avatar 360 FTIR spectrophotometer. The X-ray photoelectron spectroscopy (XPS) spectra were taken with a Thermo Scientific™ K-Alpha™^{TM+} spectrometer. Laser scanning microscopy images were taken on an LSM 710 by Zeiss. Lifetime data was collected by an Edinburgh FLS1000. X-ray diffraction pattern was taken on a Persee XD-2X/M4600.

2.3. Experimental

Synthesis of Si-O QDs: First, 0.558 g trisodium citrate was dissolved in 12 mL deionized water and bubbled with nitrogen gas to remove oxygen. Then, 3 mL DAMO was added into the above solution with vigorous stirring for 15 min, and then the solution was transferred into a Teflon-lined autoclave and heated at 200 °C for 12 h. The residual reagents were removed by dialysis (1 kDa) [25].

Synthesis of Ag NCs: First, 10 mL 50 mg/mL BSA was mixed with 10 mL 0.01 M silver nitrate and stirred for 30 min. Then, 0.6 mL 1.0 M sodium hydroxide was added into the above solution with stirring for 30 min, afterward, 4 mL 0.01 M sodium borohydride was dropped slowly into the above mixture, and stirring was continued for 2.5 h. The reddish-brown solution produced was Ag NCs [26].

Detection of H₂O₂: H₂O₂ in different concentrations was added into the Si-O QDs/Ag NCs hybrid system, and after 30 min of reaction at room temperature, the fluorescence intensities were monitored by a fluorescent spectrometer.

Detection of H₂O₂ produced by plant mitochondria: Differential velocity centrifugation was used to extract plant mitochondria from lettuce root, which referred to Ku's research [27]. Briefly, 2.0–3.0 g root sample was ground with buffer A (0.4 M sucrose, 2 mM magnesium chloride, 8 mM ethylene diamine tetraacetic acid, 4 mM cysteine, 10 mM potassium chloride, 50 mg/mL BSA, 50 mM Tris–HCl, pH = 7.6) and then transferred into a 10 mL centrifuge tube. The suspension was centrifuged at 100 rpm for 3 min. The supernatant was transferred into a new centrifuge tube and centrifuged at 600 rpm for 3 min. The supernatant was transferred into a new tube and centrifuged at 2000 rpm for 15 min, and the precipitate was discarded. The supernatant was centrifuged at 11,000 rpm for 15 min, and the precipitate was resuspended with buffer B (0.4 M sucrose, 1 mM magnesium chloride, 10 mM potassium chloride, 10 mM monopotassium phosphate, 50 mg/mL BSA, 10 mM Tris–HCl, pH = 7.2). The suspension was centrifuged at 2500 rpm for 10 min, and the precipitate was discarded. The supernatant was centrifuged at 10,000 rpm for 15 min, and the precipitate was washed twice with buffer B without BSA. All the steps were performed at low temperature (4 °C). The mitochondria suspension was centrifuged at 10,000 rpm for 15 min, and the precipitate was resuspended with 50 mM sodium silicate and incubated for 24 h at 4 °C. After discarding the mitochondria, the supernatant was added into Si-O QDs-Ag NCs solutions of different volumes, and after 30 min of reaction at room temperature, the fluorescence intensity was detected.

Detection of wound-induced H₂O₂ *in vivo*: 1 mL the Si-O QDs/Ag NCs hybrid probe was transferred into needleless syringe. And then the Si-O

QDs/Ag NCs hybrid probe was infiltrated into the leaf slowly by gently pressing the tip of the needleless syringe against the bottom of the leaf (abaxial side). The intact leaf sample was soaked in catalase solution in order to wipe out the H_2O_2 and acted as control. And the detected leaf was cut out in 40 min after injury, and was prepared for confocal scanning. And then using 20X objective lens in an inverted laser scanning confocal microscope to observe the change of fluorescence [28,29].

3. Results and discussion

3.1. Characteristics of Si-O QDs and Ag NCs

A TEM image of Si-O QDs is shown in Fig. 1a, the particles were counted taken from many such patterns, confirmed the presence of essential monodispersity. The size of particles is rather small with a narrow distribution in average size of 1.0–3.5 nm. Besides, high-resolution transmission electron microscopy (HRTEM) was applied to characterize the Si-O QDs, the particles present a characteristic spacing of 0.21 nm, which matches well with the (2 2 0) lattice planes [30,31]. XRD pattern of Si-O QDs is presented in Fig S1, it displays a broad peak at 21° (2θ), which indicates that the silica atoms are disordered [32]. According Fig. 1c, the Ag NCs shows that the particles are approximately 6 nm in size, and densely and uniformly distributed in aqueous solution. The lattice fringes of Ag NCs display interplanar spacing of 0.27 nm as shown by HRTEM, which is the evidence of the successful synthesis of Ag NCs [26]. Si-O QDs and Ag NCs both have small size which provides the possibility application on plant *in vivo*.

3.2. Structural properties of Si-O QDs

It is essential to study the chemical groups on the surface of Si-O QDs for illustrating the working mechanism of H_2O_2 detection probe basing Si-O QDs/Ag NCs system, which can be characterized by FTIR and XPS analysis. The FTIR spectrum exhibits some distinct transmittance peaks ranging from $1000\text{--}3500\text{ cm}^{-1}$ (Fig. 2a). The strong signals at $1000\text{--}1200\text{ cm}^{-1}$ are assigned to the stretching vibrations of Si - O - Si [25,31,33]. The FTIR transmittance peaks at 1586 and 3366 cm^{-1} are due to the bending vibrations and stretching vibrations of N - H bonds [26,34], respectively. The transmittance peak at 2941 cm^{-1} belongs to the unsaturated stretching vibrations of C - H bonds [35]. Furthermore, the XPS spectrum shows that Si-O QDs contain C, N, O, and Si elements (Fig. 2b). The high-resolution XPS spectrum of C 1s shows C - C (284.83 eV) bonds on the Si-O QDs surface (Fig. 2c) [35,36]; also it has C - O (286.02 eV), and C = O (287.82 eV) bonds on the surface, which makes Si-O QDs has excellent hydrophilicity. Especially, Si-O QDs may absorb citrate molecules on their surface to reduce large Si - O - Si aggregates form small particles [25,37], so that the C = O group signal appears in the XPS spectrum of Si-O QDs, but C = O groups may also come from amide groups [25,38]. Two domain peaks at 399.26 eV and 400.99 eV in the N 1s spectrum declare the presence of C - N - C and C - NH_2 bonds

(Fig. 2d). Silane molecules contribute the C - N - C groups on the surface of Si-O QDs [25,35]. The Si - O bond signal appears at 530.69 eV (Fig. 2e), while the peak centered at 532.28 eV is attributed to C - O bonds [29,36]. In the high-resolution XPS spectrum of Si (Fig. 2f), the peak at 102.39 eV is consistent with four-valent Si [25,38]. Therefore, we believe that the XPS results are in good agreement with the FTIR data. FTIR and XPS data show the Si-O QDs only have C, N, O and Si elements which are the essential nutrient elements of plant.

3.3. Structural properties of Ag NCs

FTIR and XPS also were utilized for characterizing the chemical environment of Ag NCs, the results shows that the Ag NCs also have various functional groups, as presented in Fig. 3. The peak located at around 3300 cm^{-1} corresponds to the stretching vibrations of - OH and $\square NH$. The stretching vibration at 2953 cm^{-1} represents C - H stretching. The peaks at 1652 , 1530 and 1230 cm^{-1} are assigned to the amide I, amide II, and amide III groups, respectively [39,40]. More surface functional group information about the Ag NCs can be obtained from XPS data (Fig. 3b). The C, N, O and Ag peaks are observed at around 286 , 400 , 530 and 368 eV , respectively. The high-resolution C 1s spectrum includes three peaks that are attributed to C - C (284.69 eV), C - O (285.92 eV), and C = O (287.71 eV) bonds (Fig. 4c) [26]. The N 1s and O 1s spectra exhibit main peaks at 399.83 eV and 532.16 eV , which are attributed to C - N - C and C - O, respectively (Fig. 3d&e) [26,41]. The Ag 3d spectrum clearly evidences the presence of two chemical environments for Ag. The spectrum has been fitting by considering two peaks. The first peaks, presents at 368.19 eV , corresponds to Ag 3d5. The other one is located at higher binding energy, 374.16 eV , is characteristic of Ag 3d2. The results is in good consistent with others in literatures, which verifies the existence of zero-valent Ag [24,26,41,42], and indicates the successful synthesis of Ag NCs.

3.4. The optical properties of Si-O QDs and Ag NCs

The photoluminescence (PL) excitation and emission spectra and the UV-vis absorption of Si-O QDs were measured. As shown in Fig. 4a, the optimum excitation wavelength of Si-O QDs is 360 nm , and correspondingly, Si-O QDs have an absorbance peak at 360 nm , which is due to the $n\text{-}\pi^*$ transition of C = O bonds in the Si-O QDs (Fig. 4b) [26]. The PL emission peak of the Si-O QDs is around 455 nm , and the Si-O QDs behaving an excitation-independent emission (Fig. S2a).

The photoluminescence (PL) excitation and emission spectra and the UV-vis absorption of Ag NCs were measured. As shown in Fig. S2b, the Ag NCs are excitation-independent and have broad emissions with a peak at 680 nm . The absorbance of Ag NCs ranges from 250 nm to 600 nm , and it has a shoulder peak at around 273 nm , which is attributed to tryptophan, tyrosine and disulfide from the BSA (Fig. 4b) [43,44]. The second peak at around 420 nm is due to quantum confinement effects, and it also demonstrates that BSA-Ag NCs have been synthesized [44].

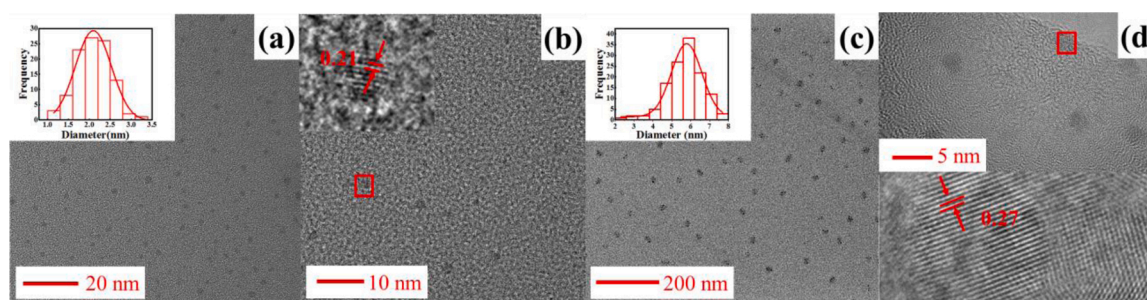


Fig. 1. (a) HRTEM image of Si-O QDs, inset: size distribution of the Si-O QDs obtained by averaging over 100 Si-O QDs HRTEM images. (b) HRTEM image of Si-O QDs, inset: enlarged HRTEM image of a single Si-O QDs. (c) TEM image of Ag NCs, inset: size distribution obtained by averaging over 100 Ag NCs HRTEM images (d) HRTEM image of Ag NCs (top), enlarged HRTEM image of a single Ag NC (down).

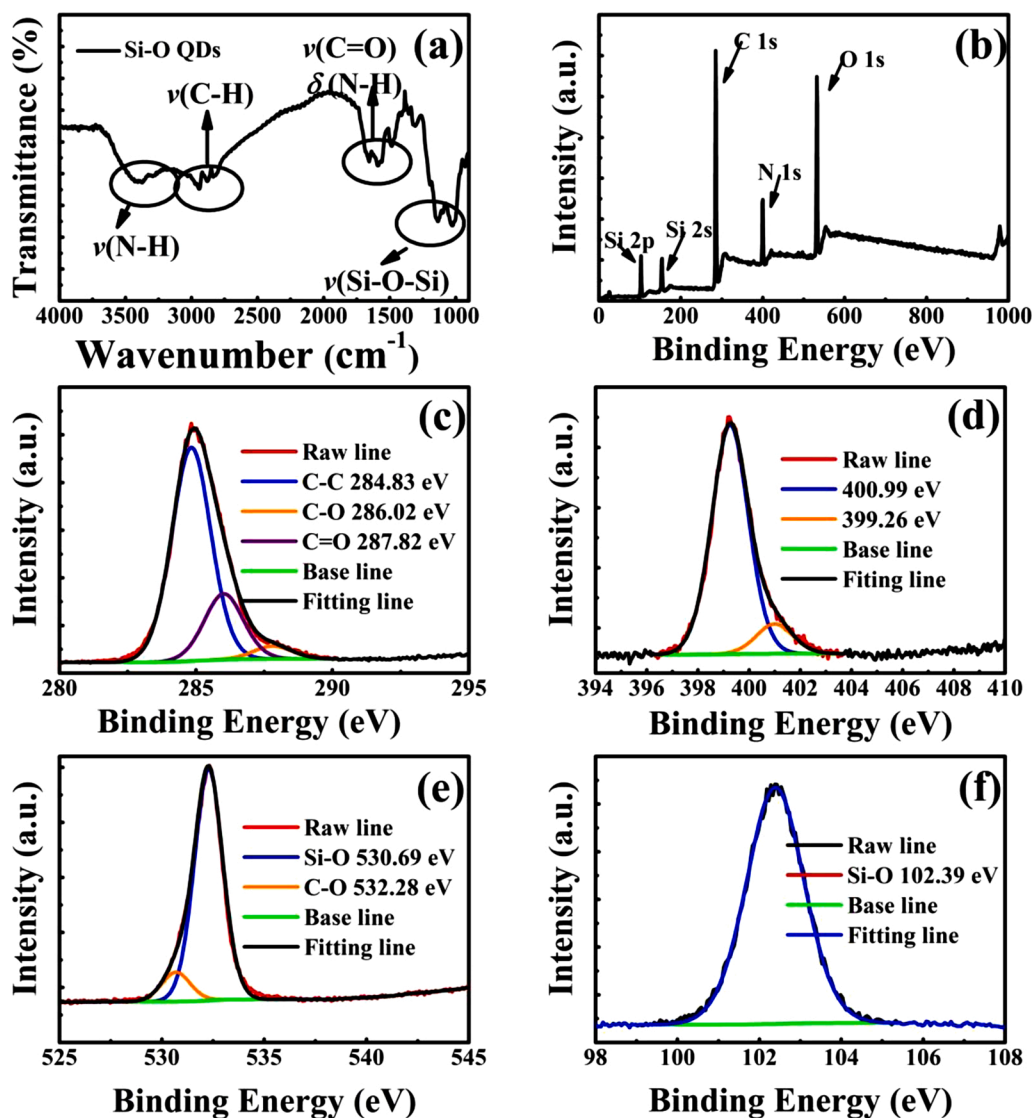


Fig. 2. (a) FTIR spectra of the Si-O QDs. (b) XPS spectra of the Si-O QDs. (c), (d), (e) and (f) High-resolution XPS spectra of C 1s, N 1s, O 1s and Si 2p, respectively.

3.5. Quenching mechanism of Si-O QDs/Ag NCs hybrid system

The UV-vis analysis of Ag NCs shows that it has absorption between 250–600 nm partly overlaying with Si-O QDs emission (Fig. 4b). Therefore, the inner-filter effect (IFE) and the fluorescent resonance energy transfer (FRET) effect are speculated for Si-O QDs emission quenching. Firstly, IFE is caused by attenuation of the excitation through absorption of other materials in solution. And FRET refers to the phenomenon of nonradiative energy transfer between two fluorescent molecules due to their close vicinity and property angular orientation. To confirm the quenching mechanism, the Si-O QDs, Ag NCs and Si-O QDs/Ag NCs hybrid system absorbance spectrum and Ag NCs absorbance spectrum are compared. The result shows that Ag NCs and Si-O QDs/Ag NCs hybrid system had same absorption peaks. (Fig. 1b), which indicates that there is no complex was formed between Si-O QDs and Ag NCs [23]. To further verify the hypothesis, IFE efficiency is estimated in Si-O QDs/Ag NCs system. The correction fluorescence wiped out IFE efficiency can be calculated based on geometry of cuvette, and the absorption characters of Si-O QDs/Ag NCs system with Eq. 1 [35,45]:

$$\frac{F_{\text{cor}}}{F_{\text{obsd}}} = \frac{2.3dA_{\text{ex}}}{1 - 10^{-dA_{\text{ex}}}} 10^{gA_{\text{em}}} \frac{2.3sA_{\text{em}}}{1 - 10^{-sA_{\text{em}}}} \quad (1)$$

where the F_{obsd} is the fluorescence of Si-O QDs at 455 nm excited by 360 nm, the F_{cor} is the corrected fluorescence of Si-O QDs. A_{ex} and A_{em} is the absorbance at maximum excitation wavelength (360 nm) and maximum emission wavelength (455 nm). d presents the cuvette width ($d = 1.00$ cm), s is the angle of excitation beam ($s = 0.10$ cm), and g is the distance from excitation light edge to the cuvette edge ($g = 0.40$ cm). The schematic of cuvette geometry parameters are shown in the Fig. S3.

The fluorescent intensity of Si-O QDs with /without Ag NCs was measured and the relative parameters were calculated, which are summarized in Table 1. The quenching effect without IFE is figured out at Fig. S4a, it illustrates that the quenching effect of IFE reaches >80% [35,46,47], which implies there are other quenching effects between Si-O QDs and Ag NCs. Therefore, the dynamic quenching effect (DQE), static quenching effect (SQE) and FRET effect were also taken into consideration. As shown in the Fig. S4b, the relationship between $F_{\text{cor},0}/F_{\text{cor}}$ and volumes of Ag NCs is nonlinearity, so that the DQE and SQD can be negligible [45,46]. Simultaneously, the FRET was investigated by observing the lifetime of Si-O QDs with or without Ag NCs. The results are shown in the Fig. S4c. The Si-O QDs lifetime is 14.41 ns, while the averaged lifetime of Si-O QDs after adding Ag NCs is 5.66 ns with bio-exponential decays. The different photoluminescence lifetimes indicate that nonradiative energy transfer or electron transfer between

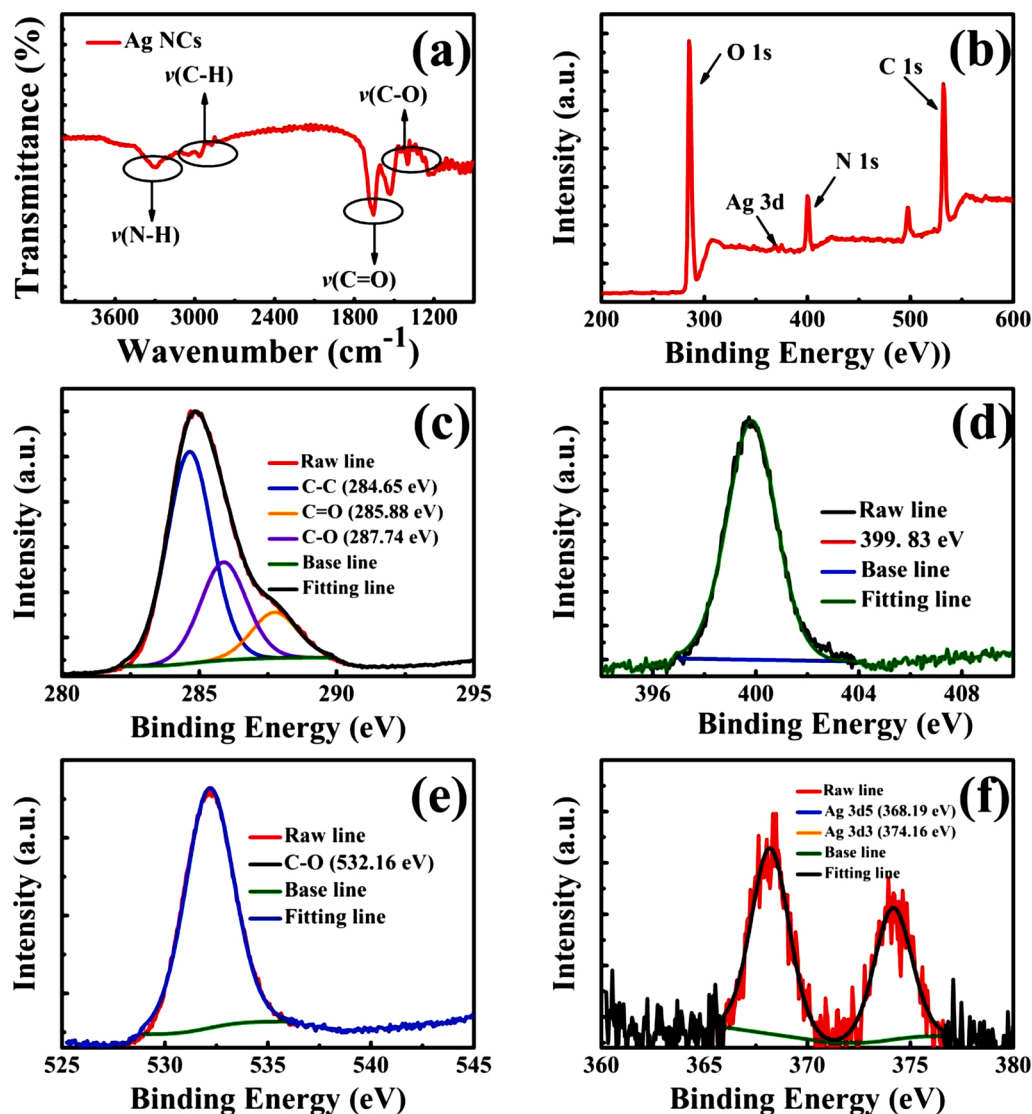


Fig. 3. (a) FTIR spectra of the Ag NCs. (b) XPS spectra of the Ag NCs. (c), (d), (e) and (f) High-resolution XPS spectra of C 1s, N 1s, O 1s and Ag 3d, respectively.

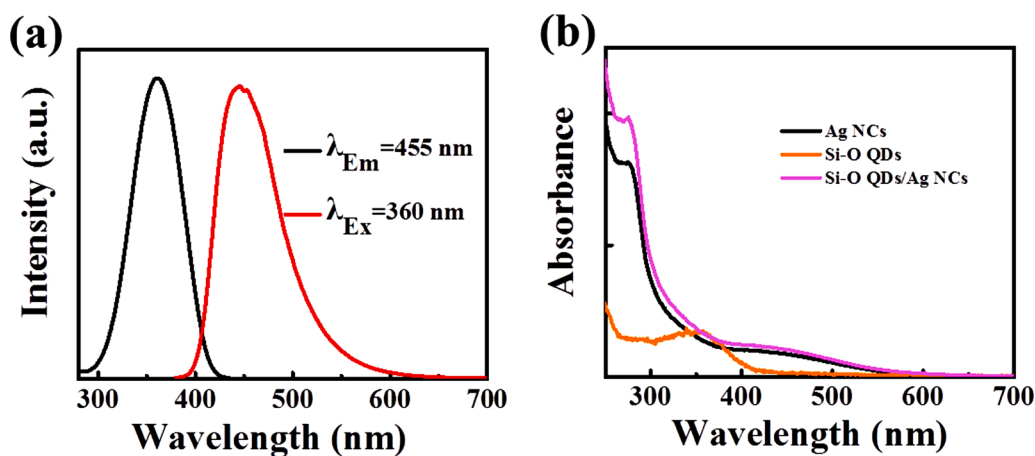


Fig. 4. (a) PL emission and excitation spectra of Si-O QDs, (b) UV-vis analysis of Si-O QDs, Ag NCs, and Si-O QDs/Ag NCs hybrid, respectively.

Si-O QDs and Ag NCs, which implies there is FRET between Si-O QDs and Ag NCs [48]. Furthermore, the FTIR spectra of Si-O QDs/Ag NCs system and Si-O QDs/Ag NCs system with H_2O_2 are shown in Fig. S5, the peak at

$1000\text{--}1200\text{ cm}^{-1}$ which is assigned to the stretching vibration of Si - O \square Si, disappears in Si-O QDs/Ag NCs system, while it can be recovered after adding H_2O_2 . Meanwhile, the peak at around 1310 cm^{-1} of C = O

Table 1
IFE efficiency of Ag NCs in acting on the fluorescence of Si-O QDs.

V(Ag NCs, μL)	A_{ex}	A_{em}	CF	F_{obsd}	F_{cor}	$F_{\text{cor,0}}/F_{\text{cor}}$
0	0.001	0.002	1.000	2248	2250.197	1.000
100	0.076	0.051	1.147	1791	2053.588	1.096
200	0.155	0.103	1.320	1489	1965.424	1.145
300	0.235	0.156	1.519	1268	1925.461	1.169
400	0.305	0.204	1.716	1114	1911.090	1.177
500	0.382	0.255	1.953	987.1	1928.245	1.167

Note: the correlated factor (CF) was calculated as $F_{\text{cor}}/F_{\text{obsd}}$, which cannot over 3; otherwise, the correction is not convincing.

vibration in Ag NCs is decreased after adding H_2O_2 in hybrid system. According to the HRTEM images of Si-O QDs/Ag NCs hybrid system with or without H_2O_2 (Fig. 5a), the aggregation morphology can be seen in Si-O QDs/Ag NCs hybrid system without H_2O_2 . While after adding H_2O_2 , two sizes of nanoparticles can be observed in HRTEM image (Fig. 5b), the lattice fringe of the small one displays interplanar spacing of 0.21 nm, which was denotes that the small one are Si-O QDs. The lattice fringe of large one is 0.27 nm, which accords with the characteristic of Ag NCs. Based on above results, Si-O QDs and Ag NCs are aggregated without H_2O_2 and separated with the presence of H_2O_2 , which fits with the disappearing and reappearing of the stretching vibration peak of Si-O-Si in the FTIR spectra. In Si-O QDs/Ag NCs hybrid system, two kinds of nanoparticles are agglomeration providing the opportunity for IFE and FRET effect to occur. After adding H_2O_2 , Si-O QDs and Ag NCs are separated, while the morphology and spacing lattice of Ag NCs are not changed. Moreover, the changes of fluorescence of Ag NCs in hybrid probe with adding different concentration of H_2O_2 are similar with the single Ag NCs reacting with H_2O_2 (Fig. 6a and Fig. 7a). It is indicating that the Si-ODs cannot enhance the oxidizability of H_2O_2 through catalyze the H_2O_2 to produce hydroxyl radical for etching Ag NCs. Therefore, according to previous related reports [26,49,50], H_2O_2 etches the protection layer (BSA) of Ag NCs by itself strong oxidizability,

and then leads to the breakage of IFE and FRET effect between Si-O QDs and Ag NCs. and then fluorescence of Si-O QDs is recovered.

3.6. Detection of H_2O_2 based on the Si-O QDs/Ag NCs probe

Firstly, to investigate the optimum concentration ratio of Si-O QDs and Ag NCs in hybrid probe system, the fluorescent intensity of different concentrations Ag NCs in hybrid probe systems was studied. The result indicates that the fluorescence intensity of Ag NCs in hybrid system would not be enhanced with the increased Ag NCs concentration above 3.47 mg/mL (Fig. S6a). Furthermore, the response of hybrid systems with different concentration ratios to a certain concentrations of H_2O_2 had also been studied, the fluorescent intensity of Ag NCs in hybrid system would not change with the increasing Ag NCs concentration in 10 mM of H_2O_2 (Fig. S6b). Therefore, 0.0066 mg/mL of Si-O QDs and 3.47 mg/mL of Ag NCs were used to establish this ratio fluorescent hybrid probe system. Besides, when the H_2O_2 concentration is lower than 0.1 mM, the fluorescent intensity of Ag NCs in this established hybrid probe remains stable (Fig. S7a). Before applying the Si-O QDs/Ag NCs system for H_2O_2 detection, the reaction time of Si-O QDs/Ag NCs system and H_2O_2 was measured, the result shows that the fluorescence of Si-O QDs/Ag NCs system is stable in 30 min after adding H_2O_2 (Fig. S7b). Therefore, H_2O_2 concentration was detected by monitoring the fluorescence of Si-O QDs/Ag NCs system in 30 min after reaction. When different concentrations of H_2O_2 are added into Si-O QDs/Ag NCs system, the fluorescent intensity of Si-O QDs is recovered progressively (Fig. 6a). The linear relationship between the ratio and H_2O_2 concentrations ranging from 0.008 to 60 mM is shown in Fig. 6b. As the concentration of H_2O_2 ranges from 0.008 to 0.1 mM, there is a good linear relationship between the intensity ratio and the H_2O_2 concentration (Fig.6c). The corresponding linear equation is as follows: $I_{455}/I_{680} = 1.232x + 0.762$ ($x = C_{\text{H}_2\text{O}_2}$; mM, $R^2 = 0.994$). Concentrations ranging from 0.1 to 2 mM, the I_{455}/I_{680} fluorescence intensity of the Si-O QDs/Ag NCs system has a good linear relationship with the H_2O_2 concentration,

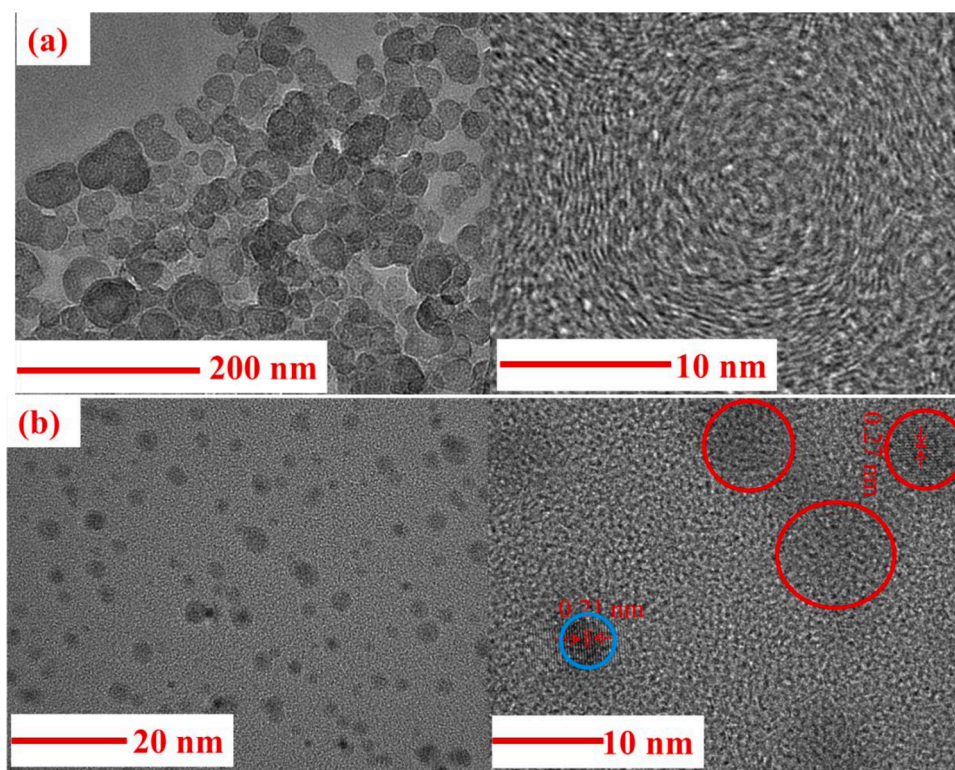


Fig. 5. (a) HRTEM image of Si-O QDs/Ag NCs hybrid system without H_2O_2 (left), enlarged HRTEM image of single particle of Si-O QDs/Ag NCs hybrid system (right). (b) HRTEM of Si-O QDs/Ag NCs with H_2O_2 (left), enlarged HRTEM image of single Si-O QDs and Ag NC, respectively (right).

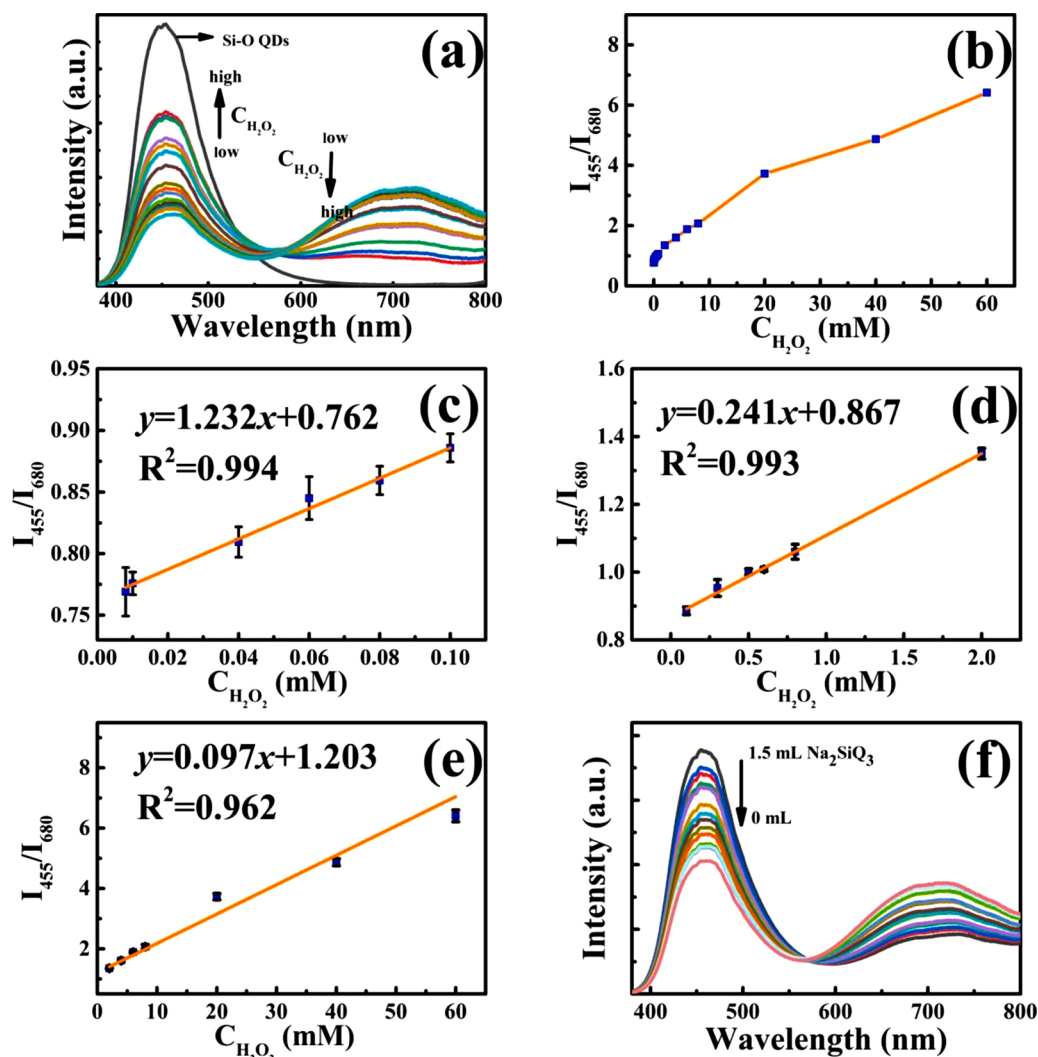


Fig. 6. (a) The PL intensity of the Si-O QDs/Ag NCs hybrid system with different concentrations of H_2O_2 , and the vertical arrow presents the concentration of H_2O_2 . (b) The relationship between the I_{455}/I_{680} fluorescence intensity and H_2O_2 concentrations from 0.008–60 mM. (c), (d) and (e) The linear relationship between the H_2O_2 concentration and the I_{455}/I_{680} fluorescence intensity in the ranges of 0.008–0.1 mM, 0.1–2 mM and 2–60 mM, respectively. (f) The PL intensity spectra of the Si-O QDs/Ag NCs system with the addition of different volumes of Na_2SiO_3 solution containing H_2O_2 produced by mitochondria.

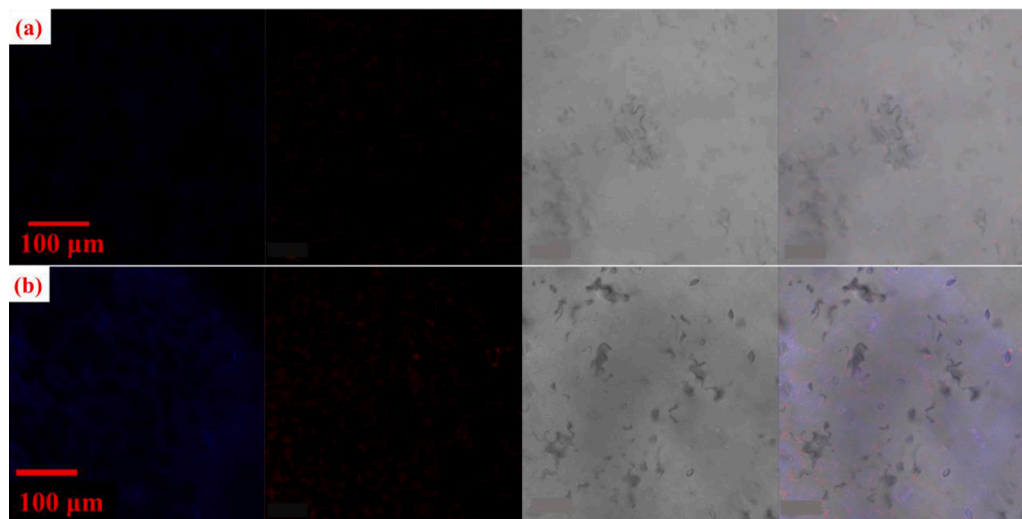


Fig. 7. (a) Laser scanning confocal microscope images of intact lettuce leaf with infiltrating Si-O QDs/Ag NCs hybrid probe system. (b) Laser scanning confocal microscope images of lettuce leaf with infiltrating Si-O QDs/Ag NCs hybrid probe system in 40 min after injury.

and the corresponding linear equation is as follows: $I_{455}/I_{680} = 0.241x + 0.867$ ($x = C_{H_2O_2}$; mM, $R^2 = 0.993$) (Fig. 6d). Furthermore, when the H_2O_2 concentration ranges from 2 to 60 mM, the corresponding linear equation is as follows: $I_{455}/I_{680} = 0.097x + 1.203$ ($x = C_{H_2O_2}$ mM, $R^2 = 0.962$) (Fig. 6e). The limit of detection (LOD) was calculated by the equation of $LOD = 3 \sigma/s$ [47,51,52], which reaches 0.0065 mM in the range of 0.008–0.1 mM ($R^2 = 0.994$). Compared with reported sensor for plant H_2O_2 detection [28,29,47,53–56], this hybrid sensor has good determination for H_2O_2 detection in plant (Table S1).

In addition, the selectivity and stability of hybrid probe were also investigated. Firstly, the pH ranging from 4 to 11 has no effect on Si-O QDs fluorescent intensity, and the different metal ions solution have less effect to hybrid probe, also the fluorescence of Si-O QDs remains stable in H_2O_2 solution with different concentrations, seen in Fig. S8a, b&c. Secondly, the fluorescent ratio (I_{455}/I_{680}) of this hybrid probe in the pH ranging from 2 to 13 was investigated, the probe shows well fluorescence stability in the range of pH from 3 to 13 (Fig S9a). Thirdly, these metal ions are the microelement for plant, and their content is low [57,58]. In order to illustrate the selectivity of this as-prepared hybrid probe in H_2O_2 detection in plant, the effects of different metal ions at 50 μ M on the ratio fluorescence of hybrid probe were investigated. The result is presented in the column chart (Fig. S9b), which demonstrates that the effects of different metal ions in plants on the fluorescence of hybrid probe could be neglected. could not affect the fluorescence of hybrid probe. The effects of metal ions on the fluorescence of Si-QDs/Ag NCs hybrid probe could be neglected (Fig. S9b). In order to apply this hybrid probe system into H_2O_2 detection in plant microenvironment, the selectivity and stability of this hybrid probe in bio-complexity condition should be investigated. According previous report, biothiols, such as cysteine (Cys), glutathione (GSH) and homocysteine (Hcy), could lead to the aggregation of Ag NCs and then the fluorescence of Ag NCs quenching [59–61]. The effects of Cys and GSH on this probe also were analyzed. These two biothiols could quench the fluorescence of Ag NCs and then the fluorescence of Si-O QDs recovery (Fig. S10a). However, the concentration of reactive oxygen species (ROS) (mainly H_2O_2) in plant could be sharply increased after high salt application and injury [28,47,62], and these ROS could lead to oxidation of the biothiols and then inactivation. Therefore, detection of high-salt induced and wound-induced H_2O_2 in plant by this Si-O QDs/Ag NCs probe could avoid the biothiols interference. The effects of Cys, GSH and different metal ions after oxidation by NaClO on the fluorescence of this hybrid system are presented in Fig. S10b&c. The fluorescence of hybrid probe with Cys and GSH after oxidation has no obvious change. The effects of these two biothiols could be neglected. The effects of different metal ions before and after oxidation on the fluorescence of hybrid probe are associated to analysis. The recovery of Si-O QDs fluorescence and decrease Ag NCs fluorescence in hybrid probe with different metal ions after oxidation were caused by the surplus NaClO which could quenching the Ag NCs depending on its strong oxidability. Therefore, the ratio fluorescent sensor basing on Si-O QDs/Ag NCs system is suitable for high-salt induced and wound-induced H_2O_2 detection of plant

3.7. Detection of H_2O_2 generated by mitochondria

Sodium silicate (Na_2SiO_3) can stimulate plant mitochondria to produce more H_2O_2 [63,64]. Therefore, Na_2SiO_3 is used to improve the H_2O_2 concentration generated from lettuce mitochondria *in vitro*, also it simulates the microenvironment in plant for probe working. Isolated mitochondria are presented in Fig. S11. After incubation, the mitochondria were removed from the Na_2SiO_3 solution, and then the solution was added into the Si-O QDs/Ag NCs system to detect the H_2O_2 concentration. After incubating, the mitochondria were wiped out from Na_2SiO_3 solution, and then the solution was added into Si-O QDs/Ag NCs system for detecting the H_2O_2 concentration. As seen in the Fig. 6f, the fluorescence of Si-O QDs in hybrid probe system is increased regularly with adding different volumes of the Na_2SiO_3 solution incubated

with mitochondria into it. When 1.5 mL solution was added, the fluorescence ratio is 4.46, and according to corresponding linear equation, the H_2O_2 concentration is calculated as 35.0 mM.

3.8. Visualized fluorescence detection of H_2O_2 in vivo

Owing to the small size of the particles in Si-O QDs/Ag NCs hybrid probe system, this hybrid probe could infiltrate into plant and detect the H_2O_2 *in vivo* without physical damage [28]. Si-O QDs/Ag NCs hybrid probe infiltrated lettuce leaf was used for determining the H_2O_2 in leaf cell *via* laser scanning confocal microscope imaging (Fig. 7a&b) [29]. The leaf sample was excited with 405 nm laser for visual fluorescent detection of H_2O_2 *in vivo*. Blue and red emission fluorescence signal was set at 420–500 nm and 600–735 nm, respectively. Due to the fluorescence of both chloroplast and Ag NCs were detected in the same range from 650–800 nm [65], the red fluorescence signal of Ag NCs cannot be isolated for detection. However, the blue fluorescence still could be the signal for H_2O_2 detection *in vivo*. In confocal images, the blue fluorescence of Si-O QDs cannot be observed in intact leaf sample which was infiltrated with Si-O QDs/Ag NCs hybrid probe, while the blue fluorescence is recovered in 40 min after the injury. Based on above results, this hybrid probe established in this research can detect wound-induced H_2O_2 qualitatively *in vivo*. Other stresses, such as salt, drought and disease, which could stimulate the plant to generate H_2O_2 [47], and these stresses induce H_2O_2 signal can be investigated by Si-O QDs/Ag NCs hybrid probe in the future. Besides, quantitative detection of H_2O_2 *in vivo* still need much research, ratio fluorescence probe could be the one of method to calculate the H_2O_2 concentration *in vivo* in the future.

4. Conclusions

In summary, an “off-on” ratio fluorescence probe basing on Si-O QDs/Ag NCs hybrid system was established. This system has good selectivity for H_2O_2 sensing within a large concentration range (from 0.008–60 mM). In particular, the system was used for sensing H_2O_2 which is generated from plant mitochondria *in vitro*. Given the small size of this probe, the system could be used as a probe to realize the visualized fluorescence of H_2O_2 qualitative detection in plant *in vivo* without complicating equipment and causing wounds on plant. Furthermore, the probe working mechanism was investigated. The results of IFE effect estimation, FTIR spectra and HRTEM images show that the quenching mechanism between Si-O QDs and Ag NCs is dependent on the IFE and FRET effect, which made the hybrid probe keep stable in microenvironment in plant. Meanwhile, after adding H_2O_2 into the hybrid system, the IFE and FRET effect between Si-O QDs and Ag NCs are broken, and thus the recovered fluorescence of Si-O QDs and the fluorescent intensity of Ag NCs could be the signal for H_2O_2 detection. This stable dual-emission ratio fluorescent probe is expected to provide an idea for plant quantitative sensing *in vivo* by calculating the fluorescent ratio.

Author contributions

Riyue Dong carried out the experimental part, analyzed the data and wrote the majority of the manuscript text. Yuying Yao and Dongna Li performed the measurements and data analysis. Haoran Zhang and Yingliang Liu provided useful suggestions and discussion concerning this manuscript. Wei Li provided the synthesis method for the nanomaterials. Maxim Molokeev modified the pictures in the manuscript. Bingfu Lei provided the idea for this work and acted as the project administrator.

Declaration of Competing Interest

The authors declare that they have no known competing financial interests or personal relationships that could have appeared to influence the work reported in this paper.

Acknowledgements

The present work was supported by the National Natural Science Foundations of China (Grant No. 21671070), the project supported by the GDUPS (2018) for Prof. Bingfu LEI, the Project for Construction of High-level University in Guangdong Province of China, the Guangzhou Science & Technology Project, China (No. 201707010033), the Special Funds for the Cultivation of Guangdong College Students' Scientific and Technological Innovation (No. 201910564035), and the National Undergraduate Innovation and Entrepreneurship Training Program granted for Riyue Dong.

Appendix A. Supplementary data

Supplementary material related to this article can be found, in the online version, at doi:<https://doi.org/10.1016/j.snb.2020.128643>.

References

- C.H. Foyer, G. Notcutt, Oxidant and antioxidant signalling in plants a re-evaluation of the concept of oxidative stress in a physiological context, *Plant Cell Environ.* 28 (8) (2005) 1056–1071, <https://doi.org/10.1111/j.1365-3040.2005.01327.x>.
- M.C. Romero-Puertas, M. Rodriguez-Serrano, F.J. Corpas, M. Gomez, L.A. Delrio, L. M. Sandalio, Cadmium-induced subcellular accumulation of O₂⁻ and H₂O₂ in pea leaves, *Plant Cell Environ.* 27 (9) (2004) 1122–1134, <https://doi.org/10.1111/j.1365-3040.2004.01217.x>.
- P.F. Tavčer, Low-temperature bleaching of cotton induced by glucose oxidase enzymes and hydrogen peroxide activators, *Biocatal. Biotransfor.* 30 (1) (2011) 20–26, <https://doi.org/10.3109/10242422.2012.644437>.
- F. Nazir, A. Hussain, Q. Fariduddin, Hydrogen peroxide modulate photosynthesis and antioxidant systems in tomato (*Solanum lycopersicum* L.) plants under copper stress, *Chemosphere* 230 (2019) 544–558, <https://doi.org/10.1016/j.chemosphere.2019.05.001>.
- K. Wei, L.Y. Wang, C.C. Zhang, L.Y. Wu, H.L. Li, H. Cheng, Endogenous nitric oxide and hydrogen peroxide detection in indole-3-butyric acid-induced adventitious root formation in *Camellia sinensis*, *J. Integr. Agr.* 17 (10) (2018) 2273–2280, [https://doi.org/10.1016/S2095-3119\(18\)62059-3](https://doi.org/10.1016/S2095-3119(18)62059-3).
- J. Bright, R. Desikan, J.T. Hancock, I.S. Weir, S.J. Neill, ABA-induced NO generation and stomatal closure in *Arabidopsis* are dependent on H₂O₂ synthesis, *Plant J.* 45 (1) (2006) 113–122, <https://doi.org/10.1111/j.1365-3113.2005.02615.x>.
- A.S. Lima, K.R. Prieto, C.S. Santos, H. Paula Valerio, E.Y. Garcia-Ochoa, A. Huerta-Robles, M. Bertotti, *In-vivo* electrochemical monitoring of H₂O₂ production induced by root-inoculated endophytic bacteria in *Agave tequilana* leaves, *Biosens. Bioelectron.* 99 (2018) 108–114, <https://doi.org/10.1016/j.bios.2017.07.039>.
- S. Chakraborty, A.L. Hill, G. Shirsekar, A.J. Afzal, G.L. Wang, D. Mackey, P. Bonello, Quantification of hydrogen peroxide in plant tissues using Amplex Red, *Methods.* 109 (2016) 105–113, <https://doi.org/10.1016/j.jymeth.2016.07.016>.
- R. Liu, S. Li, X. Yu, G. Zhang, S. Zhang, J. Yao, B. Keita, L. Nadjo, L. Zhi, Facile Synthesis of Au-nanoparticle/polyoxometalate/graphene tricomponent nanohybrids: an enzyme-free electrochemical biosensor for hydrogen peroxide, *Small* 8 (9) (2012) 1398–1406, <https://doi.org/10.1002/sml.201102298>.
- Y.W. Bao, X.W. Hua, H.H. Ran, J. Zeng, F.G. Wu, Metal-doped carbon nanoparticles with intrinsic peroxidase-like activity for colorimetric detection of H₂O₂ and glucose, *J. Mater. Chem. B* 7 (2) (2019) 296–304, <https://doi.org/10.1039/c8tb02404a>.
- L. Wang, J. Zheng, Y. Li, S. Yang, C. Liu, Y. Xiao, R. Yang, AgNP-DNA@GQDs Hybrid: New approach for sensitive detection of H₂O₂ and glucose via simultaneous AgNP etching and DNA cleavage, *Anal. Chem.* 86 (24) (2014) 12348–12354, <https://doi.org/10.1021/ac503653c>.
- Y. Zhang, S. Liu, L. Wang, X. Qin, J. Tian, W. Lu, G. Changa, X. Sun, One-pot green synthesis of Ag nanoparticles-graphene nanocomposites and their applications in SERS, H₂O₂, and glucose sensing, *RSC Adv.* 2 (2) (2012) 538–545, <https://doi.org/10.1039/c1ra00641j>.
- F. Du, Y. Min, F. Zeng, C. Yu, S. Wu, A targeted and fret-based ratiometric fluorescent nanoprobe for imaging mitochondrial hydrogen peroxide in living cells, *Small* 10 (5) (2013) 964–972, <https://doi.org/10.1002/sml.201302036>.
- P.J.S. Rana, P. Singh, P. Kar, Fluorescence alarming ON-OFF-ON switch derived from biocompatible carbon nanoparticle-hemoglobin-H₂O₂ interaction, *RSC Adv.* 6 (74) (2016) 70660–70668, <https://doi.org/10.1039/c6ra14308c>.
- S.K. Bhunia, S. Dolai, H. Sun, R. Jelinek, "On/off/on" hydrogen-peroxide sensor with hemoglobin-functionalized carbon dots, *Sens. Actuators B Chem.* 270 (2018) 223–230, <https://doi.org/10.1016/j.snb.2018.05.029>.
- Y. Yi, J. Deng, Y. Zhang, H. Li, S. Yao, Label-free Si quantum dots as photoluminescence probes for glucose detection, *Chem. Commun.* 49 (6) (2013) 612–614, <https://doi.org/10.1039/c2cc36282a>.
- F. Luo, J. Yin, F. Gao, L. Wang, A non-enzyme hydrogen peroxide sensor based on core/shell silica nanoparticles using synchronous fluorescence spectroscopy, *Microchim. Acta* 165 (1–2) (2009) 23–28, <https://doi.org/10.1007/s00604-008-0091-5>.
- L. Shang, S.J. Dong, G.U. Nienhaus, Ultra-small fluorescent metal nanoclusters: synthesis and biological applications, *Nano Today* 6 (4) (2011) 401–418, <https://doi.org/10.1016/j.nantod.2011.06.004>.
- X.J. Han, Z.T. Man, S.H. Xu, L. Cong, Y.X. Wang, X. Wang, Y.F. Du, Q.H. Zhang, S. Tang, Z.F. Liu, W. Li, A gold nanocluster chemical tongue sensor array for Alzheimer's disease diagnosis, *Colloid. Surfaces. B* 173 (2019) 478–485, <https://doi.org/10.1016/j.colsurfb.2018.10.020>.
- X. Zhang, S. Liu, X. Song, H. Wang, J. Wang, Y. Wang, J.D. Huang, J. Yu, DNA three-way junction-actuated strand displacement for miRNA detection using a fluorescence light-up Ag nanocluster probe, *Analyst.* 144 (12) (2019) 3836–3842, <https://doi.org/10.1039/c9an00508k>.
- W.W. Guo, J.P. Yuan, E.K. Wang, Oligonucleotide-stabilized Ag nanoclusters as novel fluorescence probes for the highly selective and sensitive detection of the Hg²⁺ ion, *Chem. Commun.* 23 (2009) 3395–3397, <https://doi.org/10.1039/b821518a>.
- Z.Q. Zhang, T.T. Liu, C.L. Yue, S.S. Wang, J. Ma, T. Zhou, F. Wang, X.F. Wang, G. D. Zhang, Label-free and ultrasensitive fluorescence assay for Fe³⁺ detection using DNA-Templated Ag nanoclusters, *Colloid. Surface. A* 579 (2019), 123656, <https://doi.org/10.1016/j.colsurfa.2019.123656>.
- B. Han, X. Hu, Q. Yan, J. Jiang, G. He, Ag-location-based color-tunable fluorescent AuAg nanoclusters for "turn-on" and "turn-off" detection of l-cysteine, *Sens. Actuators B.* 284 (2019) 695–703, <https://doi.org/10.1016/j.snb.2019.01.014>.
- Y.Y. Sheng, H.L. Yang, Y. Wang, L. Han, Y.J. Zhao, A.P. Fan, Silver nanoclusters-catalyzed luminol chemiluminescence for hydrogen peroxide and uric acid detection, *Talanta.* 166 (2017) 268–274, <https://doi.org/10.1016/j.talanta.2017.01.066>.
- F.G. Wu, X. Zhang, S.Q. Kai, M.Y. Zhang, H.Y. Wang, N. John, J.N. Myers, Y. X. Weng, P.D. Liu, N. Gu, C. Zhan, One-step synthesis of superbright water-soluble silicon nanoparticles with photoluminescence quantum yield exceeding 80%, *Adv. Mater. Interfaces* 2 (2015), 1500360 <https://doi.org/10.1002/admi.201500360>.
- G.Z. Yue, S.Y. Li, W. Liu, F. Ding, P. Zou, X.X. Wang, Q.B. Zhao, H.B. Rao, Ratiometric fluorescence based on silver clusters and N, Fe doped carbon dots for determination of H₂O₂ and UA: N, Fe doped carbon dots as mimetic peroxidase, *Sens. Actuators B Chem.* 287 (2019) 408–415, <https://doi.org/10.1016/j.snb.2019.02.060>.
- H.S. Ku, H.K. Pratt, A.R. Spurr, W.M. Harris, Isolation of active mitochondria from tomato fruit, *Plant Physiol.* 43 (6) (1968) 883–887, <https://doi.org/10.1104/pp.43.6.883>.
- T.T.S. Lew, V.B. Koman, K.S. Sillmore, Jun. Seo, P. Gordiichuk, S.-Y. Kwak, M. Park, M.C.-Y. Ang, D.T. Khong, M.A. Lee, M.B.C. -Park, N.-H. Chua, M.S. Strano, Real-time detection of wound-induced H₂O₂ signalling waves in plants with optical nanosensors, *Nature plant.* 6 (2020) 404–415, <https://doi.org/10.1038/s41477-020-0632-4>.
- G.M. Newkirk, H. Wu, I. Santanal, J.P. Giraldo, Catalytic scavenging of plant reactive oxygen species in vivo by anionic cerium oxide nanoparticles, *Jove-J Vis Exp* 138 (2018), e583791, <https://doi.org/10.3791/58373>.
- Y.J. Li, W. Li, H.R. Zhang, R.Y. Dong, D.N. Li, Y.L. Liu, L. Huang, B.F. Lei, Biomimetic preparation of silicon quantum dots and their phytophysiology effect on cucumber seedlings, *J. Mater. Chem. B* 7 (2019) 1107–1115, <https://doi.org/10.1039/c8tb02981d>.
- S.P. Pujari, H. Driss, F. Bannani, B. van Lagen, H. Zuilhof, One-pot gram-scale synthesis of hydrogen-terminated silicon nanoparticles, *Chem. Mater.* 30 (18) (2018) 6503–6512, <https://doi.org/10.1021/acs.chemmater.8b03113>.
- Y.J. Li, W. Li, H.R. Zhang, Y.L. Liu, L. Ma, B.F. Lei, Amplified light harvesting for enhancing Italian lettuce photosynthesis using water soluble silicon quantum dots as artificial antennas, *Nanoscale* 12 (2020) 155, <https://doi.org/10.1039/c9nr08187a>.
- A. Guleria, S. Neogy, D.K. Maurya, S. Adhikari, Blue light-emitting si quantum dots with mesoporous and amorphous features: origin of photoluminescence and potential applications, *J. Phys. Chem. C* 121 (43) (2017) 24302–24316, <https://doi.org/10.1021/acs.jpcc.7b07283>.
- M. Abdelhameed, D.R. Martir, S. Chen, W.Z. Xu, O.O. Oyene, S. Chakraborti, E. Zysman-Colman, P.A. Charpentier, Tuning the optical properties of silicon quantum dots via surface functionalization with conjugated aromatic fluorophores, *Sci. Rep.* 8 (8) (2018) 3050, <https://doi.org/10.1038/s41598-018-21181-8>.
- Y.X. Han, Y. Chen, J.J. Liu, X.Y. Niu, Y.X. Ma, S.D. Ma, X.G. Chen, Room-temperature synthesis of yellow-emitting fluorescent silicon nanoparticles for sensitive and selective determination of crystal violet in fish tissues, *Sens. Actuators B Chem.* 263 (2018) 508–516, <https://doi.org/10.1016/j.snb.2018.02.163>.
- X. Li, S. Zhang, S.A. Kulich, Y. Liu, H. Zeng, Engineering surface states of carbon dots to achieve controllable luminescence for solid-luminescent composites and sensitive Be²⁺ detection, *Sci. Rep.* 4 (2014) 4976, <https://doi.org/10.1038/srep04976>.
- Y.L. Zhong, F. Peng, F. Bao, S.Y. Wang, X.Y. Ji, L. Yang, Y.Y. Su, S.T. Lee, Y. He, Large-scale aqueous synthesis of fluorescent and biocompatible silicon nanoparticles and their use as highly photostable biological probes, *J. Am. Chem. Soc.* 35 (2013) 8350–8356, <https://doi.org/10.1021/ja4026227>.
- S. Wu, Y. Zhong, Y. Zhou, B. Song, B. Chu, X. Ji, Y. Wu, Y. Su, Y. He, Biomimetic preparation and dual-color bioimaging of fluorescent silicon nanoparticles, *J. Am. Chem. Soc.* 137 (46) (2015) 14726–14732, <https://doi.org/10.1021/jacs.5b08685>.
- B. Li, J. Li, J. Zhao, Silver nanoclusters emitting weak NIR fluorescence biomineralized by BSA, *Spectrochim. Acta. A* 134 (2015) 40–47, <https://doi.org/10.1016/j.saa.2014.06.075>.
- M. Shamsipur, F. Molaabasi, M. Sarparast, E. Roshani, Z. Vaezi, M. Alipour, K. Molaei, H. Naderi-Manesh, S. Hosseinkhani, Photoluminescence mechanisms of dual-emission fluorescent silver nanoclusters fabricated by human hemoglobin

- template: from oxidation- and aggregation-induced emission enhancement to targeted drug delivery and cell imaging, *ACS Sustain. Chem. Eng.* 6 (2018) 11123–11137, <https://doi.org/10.1021/acssuschemeng.8b02674>.
- [41] H. Sun, T. Qing, X. He, J. Shangguan, R. Jia, H. Bu, J. Huang, K. Wang, Rapid synthesis of Au/Ag bimetallic nanoclusters with highly biochemical stability and its applications for temperature and ratiometric pH sensing, *Anal. Chim. Acta* 1070 (2019) 88–96, <https://doi.org/10.1016/j.aca.2019.04.029>.
- [42] A.S. Patel, T. Mohanty, Silver nanoclusters in BSA template: a selective sensor for hydrogen peroxide, *J. Mater. Sci.* 49 (5) (2013) 2136–2143, <https://doi.org/10.1007/s10853-013-7906-4>.
- [43] W.Y. Mu, R. Yang, A. Robertson, Q.Y. Chen, A near-infrared BSA coated DNA-AgNCs for cellular imaging, *Colloid. Surfaces. B* 162 (2018) 427–431, <https://doi.org/10.1016/j.colsurfb.2017.12.023>.
- [44] Z. Chen, D. Lu, Z. Cai, C. Dong, S. Shuang, Bovine serum albumin-confined silver nanoclusters as fluorometric probe for detection of biothiols, *Luminescence* 29 (2014) 722–727, <https://doi.org/10.1002/bio.2613>.
- [45] T.D. Gauthier, E.C. Shane, W.F. Guerin, W.R. Seitz, C.L. Grant, Fluorescence quenching method for determining equilibrium constants for polycyclic aromatic hydrocarbons binding to dissolved humic materials, *Environ. Sci. Technol.* 20 (1986) 1162–1166, <https://doi.org/10.1021/es00153a012>.
- [46] W. Zhai, C. Wang, P. Yu, Y. Wang, L. Mao, Single-layer mno_2 nanosheets suppressed fluorescence of 7-hydroxycoumarin: mechanistic study and application for sensitive sensing of ascorbic acid *in vivo*, *Anal. Chem.* 86 (24) (2014) 12206–12213, <https://doi.org/10.1021/ac503215z>.
- [47] Y.J. Li, H.R. Zhang, Y.Y. Yao, T. Gong, R.Y. Dong, D.N. Li, Y.L. Liu, B.F. Lei, Promoted off-on recognition of H_2O_2 based on the fluorescence of silicon quantum dots assembled two-dimensional PEG-MnO₂ nanosheets hybrid nanoprobe, *Microchim. Acta.* 187 (2020) 347, <https://doi.org/10.1007/s00604-020-04276-w>.
- [48] H. Zong, X. Wang, X. Mu, J. Wang, M. Sun, Plasmon-enhanced fluorescence resonance energy transfer, *Chem. Rev.* 19 (2019) 818–842, <https://doi.org/10.1002/tcr.201800181>.
- [49] X.Y. Wang, G.B. Zhu, W.D. Cao, Z.J. Liu, C.G. Pan, W.J. Hu, W.Y. Zhao, J.F. Sun, A novel ratiometric fluorescent probe for the detection of uric acid in human blood based on H_2O_2 -mediated fluorescence quenching of gold/silver nanoclusters, *Talanta* 191 (2019) 46–53, <https://doi.org/10.1016/j.talanta.2018.08.015>.
- [50] W. Liu, F. Ding, Y.Y. Wang, L. Mao, R.X. Liang, P. Zou, X.X. Wang, Q.B. Zhao, H. B. Ra, Fluorometric and colorimetric sensor array for discrimination of glucose using enzymatic-triggered dual-signal system consisting of Au@Ag nanoparticles and carbon nanodots, *Sens. Actuators B Chem.* 265 (2018) 310–317, <https://doi.org/10.1016/j.snb.2018.03.060>.
- [51] X. Yan, Y. Song, C. Zhu, H. Li, D. Du, X. Su, Y. Lin, MnO_2 nanosheet-carbon dots sensing platform for sensitive detection of organophosphorus pesticides, *Anal. Chem.* 90 (2018) 2618–2624, <https://doi.org/10.1021/acs.analchem.7b04193>.
- [52] X. Yan, H.X. Li, Y. Li, X.G. Su, Visual and fluorescent detection of acetamiprid based on the inner filter effect of gold nanoparticles on ratiometric fluorescence quantum dots, *Anal. Chim. Acta* (2014) 7, <https://doi.org/10.1016/j.aca.2014.09.008>, 233463.
- [53] R. Jiménez-Pérez, L. Almagro, M.I. González-Sánchez, M.Á. Pedreño, E. Valero, Non-enzymatic screen-printed sensor based on PtNPs@polyazure A for the real-time tracking of the H_2O_2 secreted from living plant cells, *Bioelectrochemistry.* 134 (2020), 107526, <https://doi.org/10.1016/j.bioelechem.2020.107526>.
- [54] A. Prasad, A. Kumar, M. Suzuki, H. Kikuchi, T. Sugai, M. Kobayashi, P. Pospíšil, M. Tada, S. Kasai, Detection of hydrogen peroxide in Photosystem II (PSII) using catalytic amperometric biosensor, *Front. Plant Sci.* 6 (2015) 862, <https://doi.org/10.3389/fpls.2015.00862>.
- [55] P.K. Yadav, V.K. Singh, S. Chandra, D. Bano, V. Kumar, M. Talat, S.H. Hasan, Green synthesis of fluorescent carbon quantum dots from *azadirachta indica* leaves and their peroxidase-mimetic activity for the detection of H_2O_2 and ascorbic acid in common fresh fruits, *ACS Biomater. Sci. Eng.* 5 (2019) 623–632, <https://doi.org/10.1021/acsbomaterials.8b01528>.
- [56] S. Chandraa, V.K. Singh, P.K. Yadav, D. Bano, V. Kumara, V.K. Pandey, M. Talat, S. H. Hasan, Mustard seeds derived fluorescent carbon quantum dots and their peroxidase-like activity for colorimetric detection of H_2O_2 and ascorbic acid in a real sample, *Anal. Chim. Acta* (2018), <https://doi.org/10.1016/j.aca.2018.12.024>.
- [57] A. Amoozgar, A. Moammad, M.R. Sabzalian, Impact of light-emitting diode irradiation on the photosynthesis, phytochemical composition and mineral element content of lettuce cv, Grizzly, *Photosynthetica* 55 (2017) 85–95, <https://doi.org/10.1007/s11099-016-0216-8>.
- [58] D.K. Adotey, Y. Serfor-Armah, J.R. Fianko, P.O. Yeboah, Essential elements content in core vegetables grown and consumed in Ghana by instrumental neutron activation analysis, *Afr. J. Food Sci.* 3 (9) (2009) 243–249.
- [59] N. Zhang, F. Qu, H.Q. Luo, N.B. Li, Sensitive and selective detection of biothiols based on target-induced agglomeration of silver nanoclusters, *Biosens. Bioelectron.* 42 (2013) 214–218, <https://doi.org/10.1016/j.bios.2012.10.090>.
- [60] L.S. Hu, S.Q. Hu, L.Y. Guo, T. Tang, M.H. Yang, Optical and electrochemical detection of biothiols based on aggregation of silver nanoparticles, *Anal. Methods* (2016), <https://doi.org/10.1039/c6ay01295g>.
- [61] W.M. Wang, J. Li, J.L. Fan, W.M. Ning, B. Liu, C.Y. Tong, Ultrasensitive and non-labeling fluorescence assay for biothiols using enhanced silver nanoclusters, *Sens. Actuators B Chem.* 267 (2018) 174–180, <https://doi.org/10.1016/j.snb.2018.04.010>.
- [62] J. Dat, S. Vandebabeele, E. Vranová, M. Van Montagu, D. Inzé, F. Van, F. Breusegem, Dual action of the active oxygen species during plant stress responses, *Mol. Life Sci.* 57 (2000) 779–795, <https://doi.org/10.1007/s000180050041>.
- [63] L. Lyu, Y. Bi, S. Li, H. Xue, Y. Li, D.B. Prusky, Sodium silicate prime defense responses in harvested muskmelon by regulating mitochondrial energy metabolism and reactive oxygen species production, *Food Chem.* 289 (2019) 369–376, <https://doi.org/10.1016/j.foodchem.2019.03.058>.
- [64] S.S. Gill, N. Tuteja, Reactive oxygen species and antioxidant machinery in abiotic stress tolerance in crop plants, *Plant Physiol. Biochem.* 48 (2010) 909–930, <https://doi.org/10.1016/j.plaphy.2010.08.016>.
- [65] J. Li, H. Wu, I. Santana, M. Fahlgren, J.P. Giraldo, Standoff optical glucose sensing in photosynthetic organisms by a quantum dot fluorescent probe, *ACS Appl. Mater. Interfaces* 10 (34) (2018) 28279–28289, <https://doi.org/10.1021/acsaami.8b07179>.

Riyue Dong received her Master degree in agriculture from South China Agriculture University (SCAU) in 2018. And she is pursuing the PhD in College of Materials and Energy (SCAU). She research interest is nanomaterials application in plant.

Yuying Yao is an undergraduate student in College of Materials and Energy, South China Agriculture University. His research interest is application of composite nanomaterial in agriculture equipment.

Dongna Li received her Bachelor degree from South China Agriculture University in 2018. She started her Master of Chemical Engineering in SCAU. And her research is focus on nanomaterials synthesis and application.

Haoran Zhang received her PhD in 2011 in Jinan University (JNU). And currently, she is a vice-professor of College of Materials and Energy in SCAU. Her research interest is organic-inorganic hybrid compound synthesis and application.

Wei Li received her agriculture Doctor degree from s South China Agriculture University (SCAU) 2020. Her research focuses on the relationship of nanomaterials and plant physiology.

Maxim S Molochev is a professor of SB RAS, Kirensky Inst Phys, Lab Crystal Phys, Russia. And his research focuses on the crystal texture.

Yingliang Liu received his PhD in 1994 in Inorganic Chemistry from Sun Yat-Sen University. And his is a professor of College of Materials and Energy in SCAU. He is working on the synthesis and application of carbon materials and luminescent materials.

Bingfu Lei received his PhD in 2007 in Condensed Matter Physics from Changchun Institute of Optics Fine Mechanics and Physics of Chinese Academy of Sciences. And he is a professor of College of Materials and Energy in SCAU. His research focuses on luminescent nanomaterials synthesis and applying the luminescent materials in the agriculture.